In vivo endoscopic optical coherence tomography by use of a rotational microelectromechanical system probe

Peter H. Tran, David S. Mukai, Matthew Brenner, and Zhongping Chen

Department of Biomedical Engineering and Beckman Laser Institute, University of California, Irvine, Irvine, California 92612

Received December 11, 2003

A novel endoscopic optical coherence tomography probe was designed and constructed with a 1.9-mm microelectromechanical system (MEMS) motor. The new MEMS endoscopic probe design eliminates the need to couple the rotational energy from the proximal to the distal end of the probe. Furthermore, the endoscopic probe's sheath and fiber have the advantages of having a much smaller diameter and being more flexible than traditional endoscopes since no reinforcement is needed to couple the rotational torque. At the distal end, a prism mounted on a micromotor deflects the light rays to create a transverse circular-scanning pathway. Because our MEMS scanner does not require the coupling of a rotational single-mode fiber, a high scanning speed is possible while eliminating unstable optical signals caused by nonuniform coupling. © 2004 Optical Society of America

OCIS codes: 170.0170, 170.2150, 170.4500.

Optical coherence tomography (OCT) is a noninvasive, noncontact imaging modality for cross-sectional imaging of biological tissue with micrometer-scale resolution.[1] OCT was first used clinically in ophthalmology for the imaging and diagnosis of retinal disease.[2] Recently, it has been applied to image subsurface structure in skin, vessels, and the oral cavity, as well as in the respiratory, urogenital, and gastrointestinal tracts.[3] OCT is analogous to ultrasound; however, OCT uses single-scattering back-reflected infrared light rather than acoustic waves to produce higher-resolution images. Unfortunately, the penetration of OCT is generally less than 2–3 mm and requires some type of endoscope probe for internal medical diagnostics. Previous endoscopic techniques used a gear-and-shaft assembly similar to ultrasound to couple force from the motor toward the distal imaging end.[4] Such a design requires a complex rotating optical coupling joint for the single-mode fiber. Endoscopic probes with microelectromechanical system (MEMS) technology for linear scans have been demonstrated by several groups.[5,6] The MEMS probe has the advantages of small size, low cost, and excellent beam-steering capability. Currently, only linear MEMS scanning probes have been reported. However, there are many instances of medical applications for which circumferential scanning is preferred. We describe the development of a novel radial-scanning MEMS probe and present preliminary test results for *in vitro* and *in vivo* imaging based on a rotational MEMS probe.

Our rotational probe is based on a miniaturized rotational MEMS motor. A schematic diagram for the MEMS endoscopic probe is shown in Fig. 1. The outer diameter of the MEMS motor is 1.9 mm. The MEMS micromotor is mounted in a backward configuration toward the proximal endoscopic probe direction, and a 45° prism is used to deflect optical light toward the sample. Unlike a traditional catheter endoscope, the MEMS endoscope has a much simpler proximal and body design. This particular design completely eliminates the need to precisely align the fixed fiber with the rotational drive shaft. There is no rotating optical coupling joint required at the proximal end. All components are located at the distal end with a MEMS motor and micro-optical components. Since the fiber is not rotating in the body of the endoscope, a metallic sleeve for reinforcement is not necessary. For the MEMS design the body is composed of a single-mode fiber with the three-twisted wires enclosed in biocompatible polytetrafluoroethylene (PTFE) tubing that is transmissible to near-infrared light. A gradient-index (GRIN) lens with a diameter of 1 mm was used since it was readily available with 3° cleaved angles. An encapsulated probe with an outer diameter as small as 2.4 mm can be made with this MEMS micromotor.

The endoscopic probes are connected to a fiber-based OCT system for *in vitro* and *in vivo* testing as shown in Fig. 2. The OCT signal amplitude is determined by the interference fringe between a fast-scanning Fourier-domain optical delay reference line[7] and the sample arm. The broadband light source is centered at 1310 nm with a spectral bandwidth of 80 nm. In addition, phase modulators are placed on the reference arm to provide a stable carrier frequency. The data are digitized at 5 MHz, and signal processing is done as described previously.[6,8] For the endoscopic probe with the MEMS micromotor, the drive voltage is less than 1.0 V with a power of less than 60 mW.

The radial scanning is done at the distal end with a 1.9-mm MEMS motor coupled to a 0.7-mm prism. The maximum achievable speed for the current MEMS

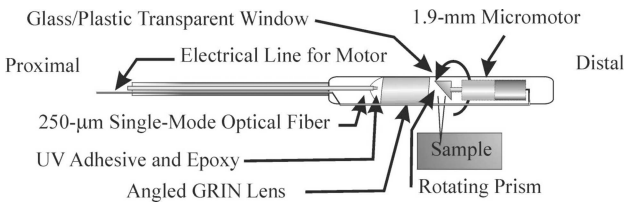

Fig. 1. Schematic endoscope MEMS probe.

0146-9592/04/111236-03$15.00/0

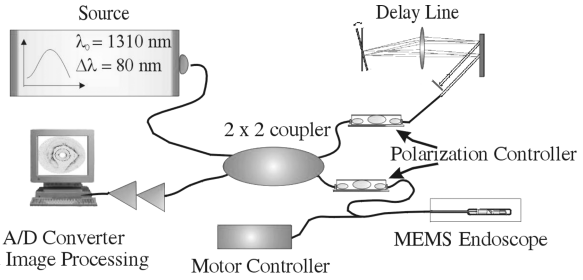

Fig. 2. Schematic of the OCT system with a MEMS probe and controller. A/D, analog-to-digital.

scanner is approximately 1 kHz. With a data acquisition rate of 5 MHz and an axial scanning rate of 1 kHz, we set the imaging scanning rate at 1 Hz. The endoscope created is shown in Fig. 3A, with a close-up of the motor and prism in Fig. 3B. Figure 3C shows the endoscopic probe on top of an infrared card in a movie-style format. As the motor rotates, the luminescence on the infrared card moves from left to right as indicated in Fig. 3C.

The MEMS endoscope signal quality is shown in Fig. 4. This figure shows the power of the back-reflected light. High constant backreflection from any optical components will degrade the performance of endoscopic OCT by reducing the detector dynamic range. For our system, the highest backreflected noise is from the PTFE sheath and not the optic component itself. The OCT signal at the interface of the GRIN lens and the fiber is eliminated by use of an angle-polished fiber along with an angled GRIN lens to reduce the dc signal and preserve the detector dynamic range. Signal reduction loss at the interface of the GRIN lens and the fiber is minimized by use of an UV adhesive to eliminate the air and glass mismatch index of refraction. The distance between the fiber–GRIN interfaces is dynamically determined by measuring the returning optical power. The working distance is set at the middle of the image or 2 mm outside the PTFE tubing (4 mm from the end of the GRIN lens). The working distance is determined by the distance between the fiber and GRIN lens and can be set based on the diameter of the lumen to be imaged. Further down the light path of the endoscopic probe is the interface between the GRIN lens and air. The internal backreflection at this interface is usually lower than the fiber–GRIN interface because the light coming out of the GRIN lens is angled relative to the normal surface. Nevertheless, a 3° angle is used for the GRIN lens to ensure low backreflection. The backreflection at the subsequent prism–air interface is less than 5%. The PTFE enclosure and the OCT target tissue signal itself are positioned after the prism signal.

For this prototype, a medical-grade PTFE tube was used to enclose the prism and GRIN lens. If all processes are constructed correctly, a strong OCT signal is obtained, which saturates the detector (see Fig. 4) when we use an IR card or mirror as a target reference. As shown in Fig. 4, more than 90% of the back-reflected photonic energy is from the sample itself. The resolution for the MEMS endoscopic probe system is approximately 13 μm at the PTFE enclosure and decreases with radial distance from the endoscopic probe. Unlike a linear-scanning endoscopic probe, which produces a constant sampling rate throughout the tissue depth, rotational endoscopic probe image resolution decreases as a function of distance from the probe source origin when the sampling rate is constant.

In vitro trachea data and *in vivo* esophageal data were obtained with the MEMS probe. For *in vitro* airway imaging, a portion of trachea was excised from a euthanized rabbit. The trachea was cut vertically and wrapped around the endoscope. Images were taken with standard *A* scanning and converted to cylindrical format in Matlab. For *in vivo* esophageal imaging, New Zealand White rabbits (2.3–4.8 kg) were anesthetized with a 2:1 mixture of ketamine HCl (100 mg/ml):xylazine (20 mg/l) at a dose of 0.75 ml/kg through a 20-gauge catheter in the marginal ear vein. The respiration rate was maintained at a rate of 30–40 breaths/min and at a tidal volume of 50 ml through a 3-mm endotracheal tube with a dual phase control respiratory pump. A mixture of 1:1 ketamine HCl (100 mg/ml):xylazine (20 mg/l) was given as necessary to maintain anesthesia.

The *in vitro* image of the rabbit trachea is shown in Fig. 5A. The tracheal cartilage ring can be seen beneath the epithelium. Layers, such as the mucosa and submucosa, can also be seen. The enlargement of Fig. 5 in the upper right-hand corner shows the location of glands (arrow). *In vivo* imaging of the esophagus is shown in Fig. 5B. The resolution for this figure is not optimized because the tissue is further from the PTFE tubing. Nevertheless, the muscularis mucosae can be seen as a dark band in Fig. 5B.

In summary, we have constructed a prototype MEMS endoscope and have demonstrated its feasibility for *in vitro* trachea and *in vivo* imaging in a rabbit

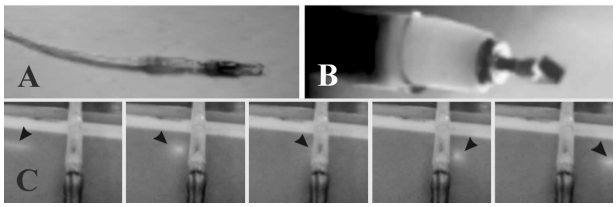

Fig. 3. Image of endoscope MEMS probe. A, Overview of the endoscope MEMS probe; B, close-up of the micromotor with prism; C, movie-style display of the endoscope on top of an IR card. Arrowheads indicate the movement of the beam as the motor rotates.

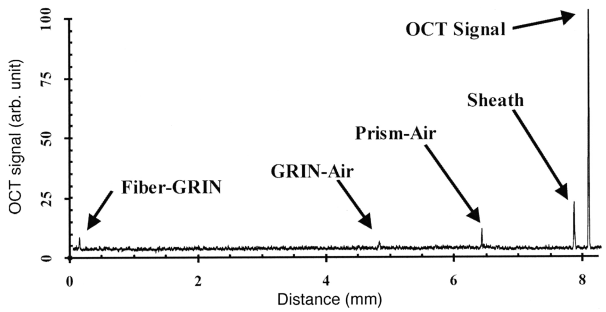

Fig. 4. Signal-to-noise ratio of the endoscope.

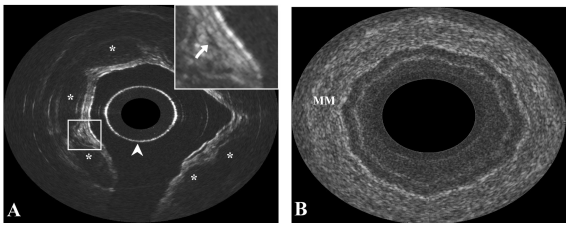

Fig. 5. A, *In vitro* image of the rabbit trachea wrapped around the endoscope. Trachea cartilage (∗) and glands (arrow in inset) can be seen. Arrowhead indicates the 2-mm PTFE tubing. B, *In vitro* image of the esophagus. MM, musculans mucosae.

esophagus. As MEMS technology is developed further, this type of radial endoscopic probe may become a preferred design for specific applications since it provides distinct advantages over previously described rotational probes. Furthermore, since high rotation speed is possible with the MEMS motor, the coupling of a linear actuator with the MEMS motor may provide three-dimensional scanning probes for high-resolution endoscopic OCT for which focus compensation can be implemented.

The authors thank Daniel Peiffer for helpful comments on this manuscript. This work was supported by research grants awarded by the National Science Foundation (BES-86924) and the National Institutes of Health (EB-00293, NCI-91717, and RR-01192). Institutional support from the Air Force Office of Scientific Research (F49620-00-1-0371) and the Beckman Laser Institute Endowment is also gratefully acknowledged. Please address all correspondence to Z. Chen at zchen@bli.uci.edu.

References

1. D. Huang, E. A. Swanson, C. P. Lin, J. S. Schuman, W. G. Stinson, W. Chang, M. R. Hee, T. Flotte, K. Gregory, C. A. Puliafito, and J. G. Fujimoto, Science **254,** 1178 (1991).
2. M. R. Lee, J. A. Izatt, E. A. Swanson, D. Huang, J. S. Schumun, C. P. Lin, C. A. Puliafito, and J. G. Fujimoto, IEEE Eng. Med. Biol. Mag. **14,** 67 (1995).
3. B. E. Bouma and G. J. Tearney, *Handbook of Optical Coherence Tomography* (Marcel Dekker, New York, 2002).
4. G. J. Tearney, S. A. Boppart, B. E. Bouma, M. E. Brezinski, N. J. Weissman, J. F. Southern, and J. G. Fujimoto, Opt. Lett. **21,** 543 (1996).
5. Y. Pan, H. Xie, and G. K. Fedder, Opt. Lett. **26,** 1966 (2001).
6. J. M. Zara, S. Yazdanfar, K. D. Rao, J. A. Izatt, and S. W. Smith, Opt. Lett. **28,** 828 (2003).
7. G. Tearney, B. Bouma, and J. Fujimoto, Opt. Lett. **22,** 1811 (1997).
8. Z. Ding, Y. Zhao, H. Ren, J. S. Nelson, and Z. Chen, Opt. Express **10,** 236 (2002), http://www.opticsexpress.org.